Supplement of Atmos. Chem. Phys., 25, 10625–10641, 2025
https://doi.org/10.5194/acp-25-10625-2025-supplement

Atmospheric Chemistry and Physics
Open Access

Supplement of

On the presence of high nitrite (NO_2^-) in coarse particles at Mt. Qomolangma

Zhongyi Zhang et al.

Correspondence to: Lei Geng (genglei@ustc.edu.cn)

Summary: 9 pages, 2 texts, 2 table, and 6 figures.

Contents of this file

S1 Isotopic analysis of TSP and soil nitrate and soil nitrite;

S2 Simulation of liquid water content and pH of TSP;

Figure S1. Wind direction and speed;

Figure S2. Time series of water-soluble inorganic ions;

Figure S3. The heatmap showing the correlations among TSP water-soluble inorganic ions;

Figure S4. Air mass back trajectories;

Figure S5. The relationships between TSP nitrite concentration with isotopic compositions;

Figure S6. The modelled TSP acidity and liquid water contents;

Table S1-S2 The uncertainties of individual ions and the nitrate isotopic signatures in TSP.

S1. Stable isotope compositions in TSP and soil nitrate

After the analysis of isotopic compositions in TSP NO_2^-, the remaining extracts of TSP samples were subsequently used for nitrate isotopic analyses via the bacterial denitrifier method(Sigman et al., 2001; Casciotti et al., 2002). Note that the nitrate isotopic composition was determined for a few TSP samples, as the extracts had been used for nitrite isotopic analysis and the available TSP amount were limited (i.e., 12h in flow rate of 30L min^{-1}). Before preparing the bacterial denitrifier method, nitrite in the TSP extracts were removed using sulfamic acid solution (0.3 mL, 1 mol L^{-1}), followed by neutralization with high-purity sodium hydroxide solution. The nitrate in extracts were also converted into N_2O with the bacterial denitrifier method and then determined following the same procedures as described above. The international nitrate isotopic reference materials (USGS32, USGS34, and USGS35) were treated along with the samples for data calibrations. The standard deviations for $\delta^{15}N$, $\delta^{18}O$, $\Delta^{17}O$ of NO_3^- reference materials were determined to be less than 0.2‰, 0.8‰, and 0.3‰, respectively. The nitrate isotopic signatures in TSP were presented in Table S1. The pre-concentrated soil extracts were also determined for nitrate isotopic compositions, and the soil nitrate isotopic compositions were presented in Table 1 in the main text.

The performance of the ion-exchange preconcentration for nitrite isotope analysis was evaluated prior to soil nitrite pretreatment in our laboratory. Briefly, 1 mL of nitrite standards (500 nmol mL^{-1}) was diluted to 150 mL and processed following the standard nitrate preconcentration protocol (Erbland et al., 2013). The isotopic analysis demonstrated the ion-exchange method was also effective for nitrite enrichment, with the differences in $\delta^{15}N$ and $\delta^{18}O$ values before and after passage through the ion-exchange resin being less than 1.6‰ across 6 replicates. Moreover, for field samples with known nitrite amount that measured by ion chromatography, the samples were subjected to resin treatment and then analyzed using the mass spectrometry after reduction into N_2O via the azide method. The peak sizes of the resulting N_2 and O_2 gases were used to estimate nitrite recovery via a calibration curve, which is established by repeating measurements of nitrite samples with known amounts varying from 30 nmol to 200 nmol. Results indicated a recovery rate of approximately 100% within analytical uncertainty.

S2. Simulation of liquid water content and pH of TSP

Particulate nitrite (as pN(III)) undergoes thermodynamic exchange processes with HONO in the atmosphere. The potential thermodynamic partitioning between pN(III) and gaseous HONO (ratio of pN(III) to HONO) in Eq.1 is investigated based on aerosol pH and liquid water content(Chen et al., 2019). The aerosol liquid water and acidity are predicted from the thermodynamic model ISORROPIA-II(Fountoukis and Nenes, 2007). The performance of ISORROPIA-II in simulation the aerosol liquid water and acidity has been well-investigated in previous studies(Guo et al., 2017; Weber et al., 2016).

$$\frac{[pN(III)]}{[HONO]}=H_{HONO}(1+\frac{k_1}{[H^+]}+\frac{[H^+]}{k_2})\times R\times T\times LWC \quad (S1)$$

with H_{HONO} representing the gaseous HONO Henry's law partitioning coefficient (49M atm^{-1}) , k_1 representing the acid dissociation constant (5.62×10^{-4} M), k_2 (≈ 0.02 M) is the equilibrium constant of between the nitroacidium ion ($H_2ONO_{(aq)}{}^+$) and $HONO_{(aq)}$ in R2 (Chen et al., 2019). The $[H^+]$ is the hydrogen ion concentration from the predicted particle pH using ISORROPIA-II. R is the gas constant, LWC is the coarse particle liquid water content.

Observations of temperature, RH (>30%), the water-soluble inorganic ions were used as inputs to calculate aerosol pH and liquid water content. The nitrite is converted to an equimolar concentration of nitrate as the chemical system in ISORROPIA-II model does not incorporate nitrite chemistry. In this study, ISORROPIA-II is run in the "forward model".

As expected, the modelled coarse particle LWC exhibits a significant contrast before and after April 30th, with mean values of 1.84 μg m^{-3} and 0.89 μg m^{-3}, respectively (Figure S6). The declines in LWC after April 30th can be attributed to decreased mass loadings of NH_4^+, SO_4^{2-} and NO_3^- with high hygroscopicity. The TSP sample is characterized by a mildly basic pH (~7.5), which is reasonable because the majority of TSP (∼3/4) in TP consists of mineral dust or lofted local soil (Kang et al., 2016; Pokharel et al., 2019).

The ratio of [pN(III)]/[HONO] was estimated based on the modelled particle pH and LWC (Text S2, using ISORROPIA thermodynamic II model) and the Eq S1. The results indicateD that the ratio of particulate NO_2^- to HONO concentration ([pN(III)]/[HONO]) varied from 4.8 to 10.6 during the campaign. Note that the ratio of [pN(III)]/[HONO] maybe overestimated since the ISORROPIA II model does not incorporate the nitrite chemistry. While concurrent measurement of gaseous HONO was unavailable in this campaign, recent filed measurement found an average of ~30 pptv of gaseous HONO in the spring of 2019 in Namco site (Wang et al., 2023), which is lower by ~5 times than our determined particulate NO_2^- concentration, analogues to the estimated [pN(III)]/[HONO] ratio.

References

Casciotti, K. L., Sigman, D. M., Hastings, M. G., Böhlke, J., and Hilkert, A.: Measurement of the oxygen isotopic composition of nitrate in seawater and freshwater using the denitrifier method, Analytical Chemistry, 74, 4905-4912, 2002.

Chen, Q., Edebeli, J., McNamara, S. M., Kulju, K. D., May, N. W., Bertman, S. B., Thanekar, S., Fuentes, J. D., and Pratt, K. A.: HONO, Particulate Nitrite, and Snow Nitrite at a Midlatitude Urban Site during Wintertime, ACS Earth and Space Chemistry, 3, 811-822, 10.1021/acsearthspacechem.9b00023, 2019.

Erbland, J., Vicars, W. C., Savarino, J., Morin, S., Frey, M. M., Frosini, D., Vince, E., and Martins, J. M. F.: Air–snow transfer of nitrate on the East Antarctic Plateau Part 1: Isotopic evidence for a photolytically driven dynamic equilibrium in summer, Atmospheric Chemistry and Physics, 13, 6403-6419, 10.5194/acp-13-6403-2013, 2013.

Fountoukis, C. and Nenes, A.: ISORROPIA II: a computationally efficient thermodynamic equilibrium model for K^+–Ca^{2+}–Mg^{2+}–NH_4^+–Na^+–SO_4^{2-}–NO_3^-–Cl^-–H_2O aerosols, Atmospheric Chemistry and Physics, 7, 4639-4659, 2007.

Guo, H., Liu, J., Froyd, K. D., Roberts, J. M., Veres, P. R., Hayes, P. L., Jimenez, J. L., Nenes, A., and Weber, R. J.: Fine particle pH and gas–particle phase partitioning of inorganic species in Pasadena, California, during the 2010 CalNex campaign, Atmospheric Chemistry and Physics, 17, 5703-5719, 10.5194/acp-17-5703-2017, 2017.

Kang, S., Chen, P., Li, C., Liu, B., and Cong, Z.: Atmospheric aerosol elements over the inland Tibetan Plateau: Concentration, seasonality, and transport, Aerosol Air Quality Research, 16, 789-800, 2016.

Pokharel, M., Guang, J., Liu, B., Kang, S., Ma, Y., Holben, B. N., Xia, X. a., Xin, J., Ram, K., Rupakheti, D., Wan, X., Wu, G., Bhattarai, H., Zhao, C., and Cong, Z.: Aerosol Properties Over Tibetan Plateau From a Decade of AERONET Measurements: Baseline, Types, and Influencing Factors, Journal of Geophysical Research: Atmospheres, 124, 13357-13374, 10.1029/2019jd031293, 2019.

Sigman, D. M., Casciotti, K. L., Andreani, M., Barford, C., Galanter, M., and Böhlke, J.: A bacterial method for the nitrogen isotopic analysis of nitrate in seawater and freshwater, Analytical chemistry, 73, 4145-4153, 2001.

Wang, J., Zhang, Y., Zhang, C., Wang, Y., Zhou, J., Whalley, L. K., Slater, E. J., Dyson, J. E., Xu, W., Cheng, P., Han, B., Wang, L., Yu, X., Wang, Y., Woodward-Massey, R., Lin, W., Zhao, W., Zeng, L., Ma, Z., Heard, D. E., and Ye, C.: Validating HONO as an Intermediate Tracer of the External Cycling of Reactive Nitrogen in the Background Atmosphere, Environ Sci Technol, 57, 5474-5484, 10.1021/acs.est.2c06731, 2023.

Weber, R. J., Guo, H., Russell, A. G., and Nenes, A.: High aerosol acidity despite declining atmospheric sulfate concentrations over the past 15 years, Nature Geoscience, 9, 282-285, 10.1038/ngeo2665, 2016.

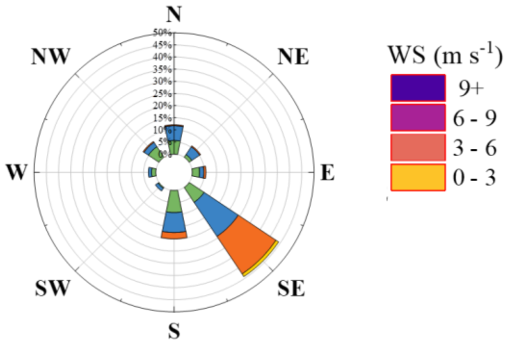

Figure S1. The wind direction and wind speed (WS, m s^{-1}) at the sampling site during the “Earth Summit Mission-2022” scientific expedition in 2022.

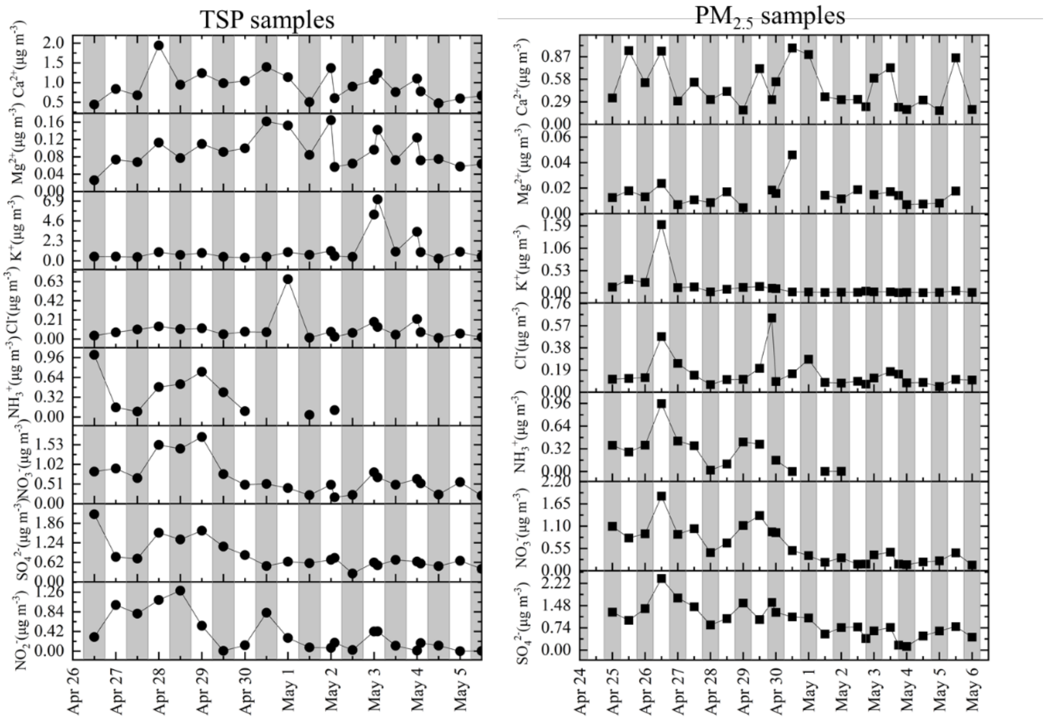

Figure S2. The time series of water-soluble ions in TSP (left panel) and $PM_{2.5}$ samples (right panel) during the “Earth Summit Mission-2022” scientific expedition in 2022.

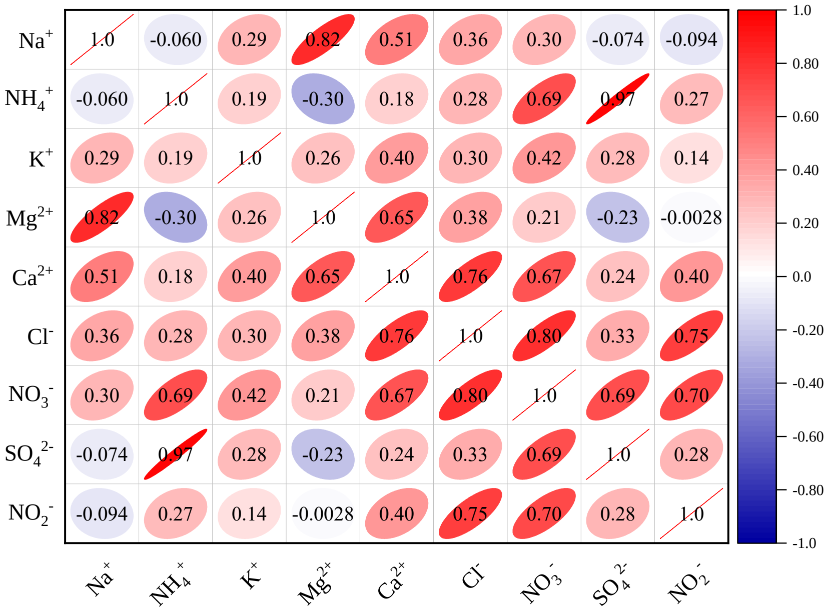

Figure S3. The correlation among the water-soluble inorganic ions in TSP samples collected samples collected at Base Camp, of Mt. Everest in spring 2022. The corresponded Pearson's r (correlation coefficient) is presented as overlapped heatmaps.

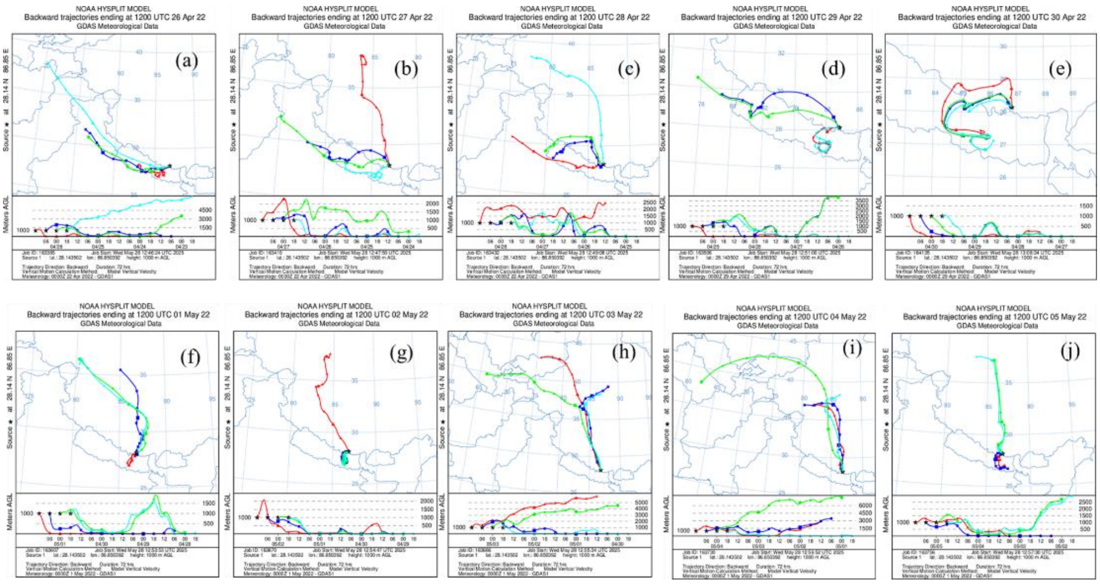

Figure S4. Similar to Figure 5 in main text. The air-mass backward trajectory was modeled at a 6 h interval each day (panels a-j) during the springtime campaign.

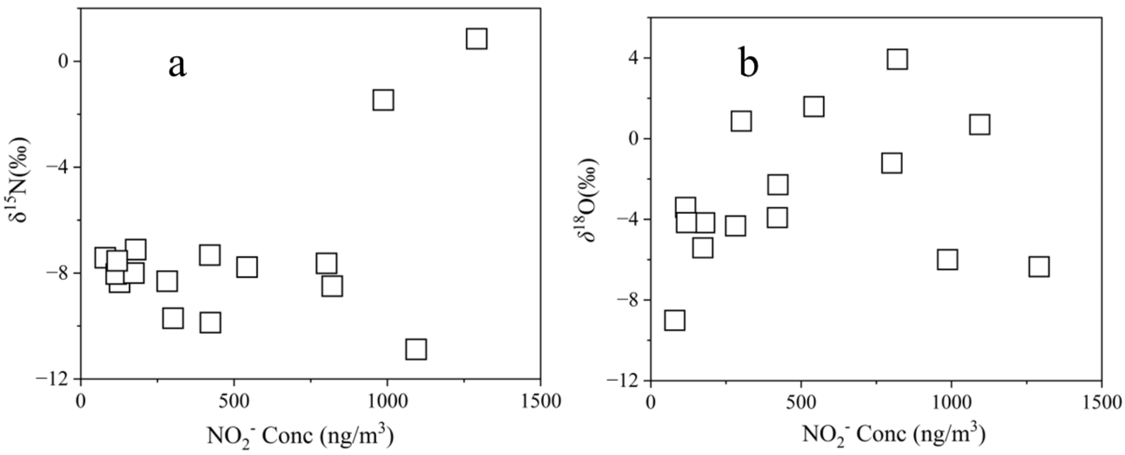

Figure S5. Relationship observed between the TSP nitrite concentration with $\delta^{15}N$ (a) and $\delta^{18}O$ (b) at Base Camp of Mt. Everest in spring 2022.

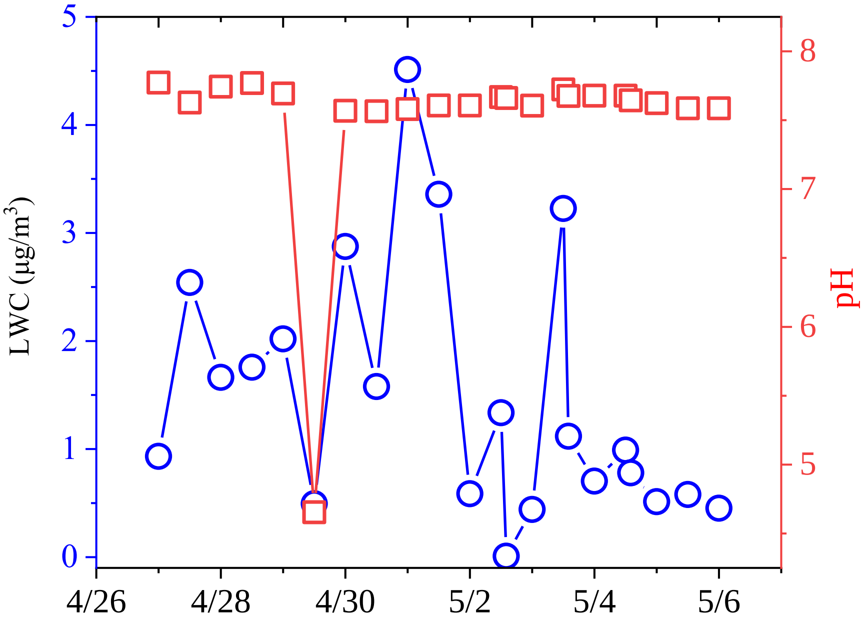

Figure S6. The predicted coarse particle liquid water content (LWC, blue circle) and acidity (red square) using the thermodynamic model ISORROPIA-II during "Earth Summit Mission" scientific expedition in spring 2022.

Table S1 The estimated uncertainty for the are concentrations ofwater-soluble ions in TSP and $PM_{2.5}$.

Species	Overall uncertainty (%)	
	TSP	$PM_{2.5}$
NO_2^-	10.8	
Cl^-	9.5	7.9
SO_4^{2-}	13.7	8.8
NO_3^-	15.3	7.5
NH_4^+	10.6	6.5
K^+	16.3	7.5
Mg^{2+}	8.3	7.5
Ca^{2+}	15.4	8.1

Table S2 The nitrate isotopic signatures in TSP collected during the campaign of "Earth Summit Mission-2022" scientific expedition.

Sample ID	Sampling period	Conc (ng/m^3)	$\delta^{15}N$(‰)	$\Delta^{17}O$(‰)
TSP-2	9:00-20:00, April 27	936	-5.2	22.1
TSP-4	9:00-20:00, April 28	1557	-8.8	18.2
TSP-5	21:00-8:00, April 27-28	1449	-0.7	29.5
TSP-6	9:00-20:00, April 29	1757	-6.3	24.0